

A phase-field model of stress effect on grain boundary migration

This article has been downloaded from IOPscience. Please scroll down to see the full text article.

2011 Modelling Simul. Mater. Sci. Eng. 19 035002

(<http://iopscience.iop.org/0965-0393/19/3/035002>)

View [the table of contents for this issue](#), or go to the [journal homepage](#) for more

Download details:

IP Address: 128.118.88.243

The article was downloaded on 24/12/2011 at 09:15

Please note that [terms and conditions apply](#).

A phase-field model of stress effect on grain boundary migration

Saswata Bhattacharyya, Tae Wook Heo, Kunok Chang and Long-Qing Chen

Department of Materials Science and Engineering, Penn State University, University Park, PA 16802, USA

E-mail: sxb57@psu.edu

Received 3 December 2010, in final form 9 February 2011

Published 3 March 2011

Online at stacks.iop.org/MSMSE/19/035002

Abstract

We developed a phase-field model to study the stress-driven grain boundary migration in elastically inhomogeneous polycrystalline materials with arbitrary elastic inhomogeneity and anisotropy. The dependence of elastic stiffness tensor on grain orientation is taken into account, and the elastic equilibrium equation is solved using the Fourier spectral iterative-perturbation method. We studied the migration of planar and curved grain boundaries under an applied stress. The relation between grain boundary migration velocity and driving force is found to be linear in the steady-state regime. Our study shows that the stress distribution depends on the relative misorientation between the grains and the nature of the applied load. As a consequence, the mechanism of grain boundary migration is different when the load is applied parallel or perpendicular to a grain boundary. The bulk mechanical driving force for grain boundary migration is provided by the difference in the level of stress in the adjoining grains which arise due to difference in elastic moduli. We further show that under certain conditions an applied stress may act as a precursor to abnormal grain growth.

(Some figures in this article are in colour only in the electronic version)

1. Introduction

Many technologically important materials are polycrystalline, containing an assembly of grains separated by grain boundaries. The temporal and spatial evolution of a grain structure takes place through migration of grain boundaries, leading to the evolution of microstructure characteristics such as grain size, morphology and topology. As the microstructure controls the physical and mechanical properties of a material, grain boundary migration and grain growth kinetics has always been a subject of intense interest. Although most of the studies on grain growth are focused on curvature-driven grain boundary migration [1], there has been

increasing interest in the effect of external loads such as applied stress, magnetic and electric fields. For example, there have been several experimental studies to understand the stress-driven migration of both low and high-angle grain boundaries [2–6]. Winning *et al* studied the motion of planar and curved tilt boundaries under the influence of mechanical shear stress [4, 5]. They observed that externally imposed stress can induce the motion of both low- and high-angle grain boundaries. Based on the measured activation enthalpies, they attributed the motion of planar grain boundaries to the movement of grain boundary dislocations. Their study shows that the mobility of grain boundaries does not depend on the angle of misorientation except for a sharp change during the transition from low- to high-angle boundaries.

There have been a number of atomistic molecular dynamics (MD) simulations of stress-induced grain boundary migration. Schonfelder *et al* employed MD to study the intrinsic migration behavior of flat, high-angle grain boundaries under an applied strain [7]. They concluded that the velocity-driving force relationship is linear up to 4% of applied strain. Using MD simulations, Zhang *et al* studied elastically driven migration of flat grain boundaries in a system where the driving force for boundary migration does not change with time [8]. They determined the activation energy for grain boundary migration and the mobility of a grain boundary at different temperatures. They observed that the grain boundary velocity is a nonlinear function of the driving force, especially at low temperatures. Based on MD simulations of grain boundary motion under a shear stress, Ivanov and Mishin concluded that the stress–velocity relation is nonlinear at low temperature and high velocities and becomes approximately linear at high temperatures and low velocities [9]. More recently, various MD simulation schemes have been developed and used to study grain boundary migration in bicrystals. Different types of driving forces, such as curvature driving force originating from capillary effect, difference in the strain energy densities between grains, an artificial driving force by changing the potential energy of atoms, and random walk of planar grain boundaries induced by thermal fluctuations, have been employed to study the migration of grain boundaries (see [10] for an excellent overview of the MD based techniques).

MD simulations are ideal for determining the mobility of a grain boundary under applied stress and atomistic mechanisms of grain boundary migration. However, the computational cost and the length and time scales involved in MD make it difficult to directly simulate the migration of grain boundaries in multigrain systems, i.e. grain growth. On the other hand, the phase-field method has emerged as a powerful tool for studying microstructural evolution at the mesoscale (see reviews [11–13] for detail). They are continuum models and can provide useful insight into the mesoscale mechanisms of grain boundary migration under an applied stress. These models have been extensively used to study curvature-driven grain growth [14–17] and the effect of elastic stresses on microstructural evolution during coherent phase transformations in solids (see [13] and references therein). However, many of the existing models use the homogeneous elastic modulus approximation. Although homogeneous modulus approximation is sufficient to explain several morphological features such as shape change of coherent inclusions with size and their alignment along elastically favorable directions, the assumption is not valid when the microstructure exhibits large elastic inhomogeneity. For example, to study stress effect on grain growth, we need to take into account the dependence of the elastic stiffness tensor on the orientation of each grain constituting the polycrystal. In this paper, our aim is to establish a phase-field model in which both curvature and mechanical driving forces are taken into account. Such a model will be useful to study microstructural evolution in polycrystalline systems under applied load.

Recently there have been several approaches to treat the effect of elastic inhomogeneity in solids [18–27] in phase-field models. Jou *et al* studied microstructural evolution in elastically inhomogeneous two-dimensional binary alloy [18] where they solved the elastic

field for arbitrarily shaped precipitates using the boundary integral method together with a small scale preconditioner. Moulinec and Suquet proposed an efficient algorithm based on Fourier series to compute the overall response of nonlinear composites with complex microstructures [19]. In their method they calculated Green's function of linear elastic and homogeneous comparison material and used an iterative procedure to solve the mechanical equilibrium equation when elastically inhomogeneous constituents are considered. They further improved their iterative method using a scheme based on augmented Lagrangian method and applied their scheme to calculate the response of linear and nonlinear composites with arbitrary ratio of elastic constants between the constituent phases [20, 21]. Lebensohn presented a formulation to compute the local response of elastic and viscoplastic anisotropic 3D polycrystals based on fast Fourier transform (FFT) algorithm [22]. His formulation is an extension of the FFT method proposed by Suquet and co-workers [19–21] and takes into account elastic heterogeneity arising due to directional properties of grains with different crystallographic orientations. Zhu *et al* studied microstructural evolution during phase separation and coarsening in systems with strong elastic inhomogeneity [27]. They solved the two-dimensional inhomogeneous elastic equilibrium equations using the conjugate gradient method. Wang *et al* developed a phase-field microelasticity theory to model elastically and structurally inhomogeneous solids [23, 24]. Their theory is based on the estimation of strain energy of an elastically inhomogeneous solid by numerically computing the effective stress free strain for an equivalent elastically homogeneous system. Hu and Chen developed an iterative-perturbation method based on Fourier spectral implementation to study microstructural evolution in elastically inhomogeneous and anisotropic systems [25]. Yu *et al* demonstrated the efficiency of the iterative-perturbation scheme through numerical experiments and mathematical justification [26].

In this study, we extended the iterative-perturbation method developed by Hu and Chen [25] to compute stress distribution in elastically inhomogeneous polycrystals. This allows us to compute the stress distribution for any arbitrary structurally and elastically inhomogeneous microstructures. We integrated our method with the multi-order parameter phase-field model for grain growth developed by Fan and Chen [15] to study stress-driven grain boundary migration. Since our main objective is to develop the phase-field model for studying microstructural evolution in elastically inhomogeneous polycrystalline systems, we focus on simple examples to test our approach. However, our model can be used to study grain growth and texture evolution in complex polycrystalline systems in two and three dimensions under applied load.

The paper is organized as follows: in section 2 we describe our phase-field model to study stress-driven grain boundary migration in elastically inhomogeneous polycrystals. In section 3 we present the salient results from our study and summarize our important findings in section 4.

2. Formulation

2.1. Elastic stress distribution in polycrystals

In the phase-field model developed for grain growth [15, 28], a polycrystalline microstructure is described using a set of Q continuous, non-conserved order parameter fields $\eta_g(\mathbf{r}, t)$ ($g = 1 \dots Q$). The order parameter fields represent grains of a given crystallographic orientation.

In a polycrystalline material, the elastic moduli depend on the relative orientation of different grains and hence are always inhomogeneous. Since the grains are rotated with respect to a fixed coordinate system, the elastic stiffness tensor for each grain is obtained by

transforming the tensor with respect to the fixed coordinate system. Let C_{ijkl} represent the stiffness tensor for a single grain in a fixed reference frame. Then, the position-dependent elastic stiffness tensor for the entire polycrystal in terms of the order parameter fields is given by

$$C_{ijkl}(\mathbf{r}) = \sum_g \Phi_g(\mathbf{r}) a_{ip}^g a_{jq}^g a_{kr}^g a_{ls}^g C_{pqrs}, \quad (1)$$

where a_{mn} ($m, n = 1 \dots 3$) is the transformation matrix representing the rotation of the coordinate system defined on a given grain 'g' with respect to the fixed reference frame. We use a function $\Phi_g(\mathbf{r}) = \eta_g^2(\mathbf{r})$ to distinguish between the grain interior and the grain boundaries. The function is chosen arbitrarily with the assumption that the grain boundary is elastically softer than the interior. C_{pqrs} denotes the stiffness tensor of the reference medium. a_{ij} is expressed in terms of the Euler angles θ , ψ and ζ (in three dimensions):

$$\begin{aligned} a_{11} &= \cos \theta \cos \zeta - \sin \theta \sin \zeta \cos \psi, & a_{12} &= \sin \theta \cos \zeta + \cos \theta \sin \zeta \cos \psi, \\ a_{13} &= \sin \zeta \sin \psi, & a_{21} &= -\cos \theta \sin \zeta - \sin \theta \cos \zeta \cos \psi, \\ a_{22} &= -\sin \theta \sin \zeta + \cos \theta \cos \zeta \cos \psi, & a_{23} &= \cos \zeta \sin \psi, \\ a_{31} &= \sin \theta \sin \psi, & a_{32} &= -\cos \theta \sin \psi, & a_{33} &= \cos \psi, \end{aligned} \quad (2)$$

where $0 \leq \theta \leq 2\pi$, $0 \leq \psi \leq \pi$, $0 \leq \zeta \leq 2\pi$. In addition, the elastic constants may depend on additional variables such as concentration and order parameters. However, in this work, we focus on the effect of elastic inhomogeneity stemming from the different grain orientations in a grain structure.

It should be noted that the phase-field model takes into account all the five degrees of freedom of the grain boundaries. Misorientation of the grain boundaries is specified by assigning three Euler angles to each grain. Since our phase-field model is based on free energy minimization with respect to the grain order parameters, the inclinations of the grain boundaries are automatically determined during the simulations. Hence our model does not require additional parameters to describe the inclinations of the grain boundaries.

The spatially dependent elastic stiffness tensor, $C_{ijkl}(\mathbf{r})$, can be written as a sum of a constant homogeneous part C_{ijkl}^0 and a position-dependent inhomogeneous perturbation $C'_{ijkl}(\mathbf{r})$. When the homogeneous part is assumed to be isotropic, the homogeneous elastic constants can be expressed in terms of two independent elastic constants, bulk modulus K and shear modulus μ :

$$C_{ijkl}^0 = C_{ijkl}^{iso} = K \delta_{ij} \delta_{kl} + \mu \left(\delta_{ik} \delta_{jl} + \delta_{il} \delta_{jk} - \frac{2}{d} \delta_{ij} \delta_{kl} \right), \quad (3)$$

where d represents the dimensionality of the system and δ_{ij} is Kronecker's delta function.

Otherwise, the homogeneous part can also be approximated as the mean between the maximum and minimum values of $C_{ijkl}(\mathbf{r})$:

$$C_{ijkl}^0 = \frac{1}{2} (\max(C_{ijkl}(\mathbf{r})) + \min(C_{ijkl}(\mathbf{r}))). \quad (4)$$

The remaining elastic constants are treated as inhomogeneous perturbation. Thus $C_{ijkl}(\mathbf{r})$ can be rewritten as

$$C_{ijkl}(\mathbf{r}) = C_{ijkl}^0 + \left(\sum_g \eta_g^2(\mathbf{r}) a_{ip}^g a_{jq}^g a_{kr}^g a_{ls}^g C_{pqrs} - C_{ijkl}^0 \right), \quad (5)$$

where $g = 1 \dots Q$ and a_{ij}^g represents the transformation matrix for grain g defined with respect to a fixed coordinate system.

Let $\epsilon_{ij}(\mathbf{r})$ denote the total strain measured with respect to a reference undeformed lattice. Then, assuming linear elasticity, the local stress $\sigma_{ij}(\mathbf{r})$ is given as

$$\sigma_{ij}(\mathbf{r}) = (C_{ijkl}^0 + C'_{ijkl}(\mathbf{r}))(\epsilon_{kl}(\mathbf{r}) - \epsilon_{kl}^0(\mathbf{r})). \quad (6)$$

Here, the position-dependent eigenstrain tensor $\epsilon_{ij}^0(\mathbf{r})$ is a local plastic strain which can arise from many different processes such as phase transformations, thermal expansion mismatch and plastic deformation.

To obtain the local elastic field, we solve the mechanical equilibrium equation

$$\frac{\partial \sigma_{ij}}{\partial r_j} = 0, \quad \text{i.e.} \quad \nabla_j C_{ijkl}(\mathbf{r})(\epsilon_{kl}(\mathbf{r}) - \epsilon_{kl}^0(\mathbf{r})) = 0. \quad (7)$$

The total strain $\epsilon_{kl}(\mathbf{r})$ can be expressed as a sum of homogeneous and heterogeneous strains [29]:

$$\epsilon_{ij}(\mathbf{r}) = \bar{\epsilon}_{ij} + \delta\epsilon_{ij}(\mathbf{r}), \quad (8)$$

where the homogeneous strain $\bar{\epsilon}_{ij}$ is defined such that

$$\int \delta\epsilon_{ij}(\mathbf{r}) d^3r = 0. \quad (9)$$

The heterogeneous strain field $\delta\epsilon_{ij}(\mathbf{r})$ is defined as

$$\delta\epsilon_{ij}(\mathbf{r}) = \frac{1}{2} \left(\frac{\partial u_i(\mathbf{r})}{\partial r_j} + \frac{\partial u_j(\mathbf{r})}{\partial r_i} \right), \quad (10)$$

where $u_i(\mathbf{r})$ denotes the i th component of displacement field.

Using equations (8) and (10) in equation (7) we obtain

$$\nabla_j C_{ijkl}(\mathbf{r}) \left[\bar{\epsilon}_{kl} + \frac{1}{2} \left(\frac{\partial u_k(\mathbf{r})}{\partial r_l} + \frac{\partial u_l(\mathbf{r})}{\partial r_k} \right) - \epsilon_{kl}^0(\mathbf{r}) \right] = 0. \quad (11)$$

Equation (11) can be rewritten using equation (5) as

$$\begin{aligned} \nabla_j \left[C_{ijkl}^0 + \left(\sum_g \eta_g^2(\mathbf{r}) a_{ip}^g a_{jq}^g a_{kr}^g a_{ls}^g C_{pqrs} - C_{ijkl}^0 \right) \right] \\ \times \left[\bar{\epsilon}_{kl} + \frac{1}{2} \left(\frac{\partial u_k(\mathbf{r})}{\partial r_l} + \frac{\partial u_l(\mathbf{r})}{\partial r_k} \right) - \epsilon_{kl}^0(\mathbf{r}) \right] = 0. \end{aligned} \quad (12)$$

Rearranging and simplifying equation (12), we obtain

$$\begin{aligned} C_{ijkl}^0 \frac{\partial^2 u_k}{\partial r_j \partial r_l} = \nabla_j \left[\left(\sum_g \eta_g^2(\mathbf{r}) a_{ip}^g a_{jq}^g a_{kr}^g a_{ls}^g C_{pqrs} \right) (\epsilon_{kl}^0(\mathbf{r}) - \bar{\epsilon}_{kl}) \right] \\ - \frac{\partial}{\partial r_j} \left[\left(\sum_g \eta_g^2(\mathbf{r}) a_{ip}^g a_{jq}^g a_{kr}^g a_{ls}^g C_{pqrs} - C_{ijkl}^0 \right) \frac{\partial u_k}{\partial r_l} \right]. \end{aligned} \quad (13)$$

Following Hu and Chen [25], we implement an iterative-perturbation scheme to solve equation (13) as follows:

Zeroth-order approximation. We assume the elastic constants to be homogeneous and solve the mechanical equilibrium equation. In other words, $C'_{ijkl}(\mathbf{r})$ is set to zero in equation (13). Thus we obtain

$$C_{ijkl}^0 \frac{\partial^2 u_k(\mathbf{r})}{\partial r_j \partial r_l} = C_{ijkl}^0 \nabla_j (\epsilon_{kl}^0(\mathbf{r})). \quad (14)$$

The zeroth-order displacement field is obtained by solving equation (14) in Fourier space:

$$\tilde{u}_k^0(\mathbf{k}) = -IG_{ik}(\mathbf{k})k_j\tilde{\sigma}_{ij}^0(\mathbf{k}), \quad (15)$$

where $\tilde{u}_k^0(\mathbf{k})$ and $\tilde{\sigma}_{ij}^0(\mathbf{k})$ are Fourier transforms of $u_k^0(\mathbf{r})$ and $\sigma_{ij}^0(\mathbf{r})$, respectively, \mathbf{k} is the reciprocal lattice vector, k_j is the j th component of \mathbf{k} , $G_{ik}(\mathbf{k})$ is the Green tensor whose inverse is defined as $G_{ik}^{-1}(\mathbf{k}) = C_{ijkl}^0 k_j k_l$, and $\sigma_{ij}^0(\mathbf{r}) = C_{ijkl}^0 \epsilon_{ij}^0(\mathbf{r})$.

First-order approximation. We substitute the zeroth-order displacement solution in the nonlinear term in equation (13) and rearrange the terms:

$$C_{ijkl}^0 \frac{\partial^2 u_k^1(\mathbf{r})}{\partial r_j \partial r_l} = \nabla_j \left\{ \left(\sum_g \eta_g^2(\mathbf{r}) a_{ip}^g a_{jq}^g a_{kr}^g a_{ls}^g C_{pqrs} \right) (\epsilon_{kl}^o(\mathbf{r}) - \bar{\epsilon}_{kl}) \right\} - \frac{\partial}{\partial r_j} \left[\left(\sum_g \eta_g^2(\mathbf{r}) a_{ip}^g a_{jq}^g a_{kr}^g a_{ls}^g C_{pqrs} - C_{ijkl}^0 \right) \frac{\partial u_k^o(\mathbf{r})}{\partial r_l} \right]. \quad (16)$$

The solution $u_k^1(\mathbf{r})$ is obtained in Fourier space:

$$\tilde{u}_k^1(\mathbf{k}) = -IG_{ik}(\mathbf{k})k_j \left[\begin{array}{c} \left(\sum_g \eta_g^2(\mathbf{r}) a_{ip}^g a_{jq}^g a_{kr}^g a_{ls}^g C_{pqrs} \right) (\epsilon_{kl}^o(\mathbf{r}) - \bar{\epsilon}_{kl}) \\ - \left(\sum_g \eta_g^2(\mathbf{r}) a_{ip}^g a_{jq}^g a_{kr}^g a_{ls}^g C_{pqrs} - C_{ijkl}^0 \right) \frac{\partial u_k^o(\mathbf{r})}{\partial r_l} \end{array} \right]_k. \quad (17)$$

Higher-order approximation. The higher-order solutions for $u_k(\mathbf{r})$ are derived in a similar way as the first-order approximation.

$$C_{ijkl}^0 \frac{\partial^2 u_k^n(\mathbf{r})}{\partial r_j \partial r_l} = \nabla_j \left\{ \left(\sum_g \eta_g^2(\mathbf{r}) a_{ip}^g a_{jq}^g a_{kr}^g a_{ls}^g C_{pqrs} \right) (\epsilon_{kl}^o(\mathbf{r}) - \bar{\epsilon}_{kl}) \right\} - \frac{\partial}{\partial r_j} \left[\left(\sum_g \eta_g^2(\mathbf{r}) a_{ip}^g a_{jq}^g a_{kr}^g a_{ls}^g C_{pqrs} - C_{ijkl}^0 \right) \frac{\partial u_k^{n-1}(\mathbf{r})}{\partial r_l} \right]. \quad (18)$$

The solution $u_k^n(\mathbf{r})$ is obtained using Fourier transforms.

$$\tilde{u}_k^n(\mathbf{k}) = -IG_{ik}(\mathbf{k})k_j \left[\begin{array}{c} \left(\sum_g \eta_g^2(\mathbf{r}) a_{ip}^g a_{jq}^g a_{kr}^g a_{ls}^g C_{pqrs} \right) (\epsilon_{kl}^o(\mathbf{r}) - \bar{\epsilon}_{kl}) \\ - \left(\sum_g \eta_g^2(\mathbf{r}) a_{ip}^g a_{jq}^g a_{kr}^g a_{ls}^g C_{pqrs} - C_{ijkl}^0 \right) \frac{\partial u_k^{n-1}(\mathbf{r})}{\partial r_l} \end{array} \right]_k. \quad (19)$$

The number of iterations required to refine the displacement solution depends on the desired accuracy for the problem. Generally, except for cases with extremely large elastic inhomogeneity, fewer than three iterations are required to achieve convergence of the displacement solution.

2.2. Calculation of homogeneous strain

When a system is under a constant strain, the homogeneous strain is equal to the applied strain. However, when the boundaries of the system are allowed to relax, the homogeneous strain is obtained by minimizing the total elastic energy. We derive a general expression for

homogeneous strain assuming that a constant stress is applied to the system. When the system is subjected to an applied stress σ_{ij}^a , the total elastic energy of the system is given by [30]

$$F_{el} = \frac{1}{2} \int_V C_{ijkl}(\mathbf{r}) [\bar{\epsilon}_{ij} + \delta\epsilon_{ij}(\mathbf{r}) - \epsilon_{ij}^0(\mathbf{r})] [\bar{\epsilon}_{kl} + \delta\epsilon_{kl}(\mathbf{r}) - \epsilon_{kl}^0(\mathbf{r})] dV - \int_V \sigma_{ij}^a \bar{\epsilon}_{ij} dV. \quad (20)$$

Minimization of total elastic energy with respect to homogeneous strain yields

$$\begin{aligned} \frac{\partial F_{el}}{\partial \bar{\epsilon}_{ij}} &= 0, \\ \Rightarrow \int_V C_{ijkl}(\mathbf{r}) \bar{\epsilon}_{kl} dV + \int_V C_{ijkl}(\mathbf{r}) \delta\epsilon_{kl}(\mathbf{r}) dV - \int_V C_{ijkl}(\mathbf{r}) \epsilon_{kl}^0(\mathbf{r}) dV - V \sigma_{ij}^a &= 0, \\ \Rightarrow \sigma_{ij}^a &= \bar{\epsilon}_{kl} \frac{1}{V} \int_V C_{ijkl}(\mathbf{r}) dV + \frac{1}{V} \int_V C_{ijkl}(\mathbf{r}) \delta\epsilon_{kl}(\mathbf{r}) dV - \frac{1}{V} \int_V C_{ijkl}(\mathbf{r}) \epsilon_{kl}^0(\mathbf{r}) dV, \\ \Rightarrow \bar{\epsilon}_{kl} &= \langle S_{ijkl} \rangle (\sigma_{ij}^a + \langle \sigma_{ij}^0 \rangle - \langle \delta\sigma_{ij} \rangle), \end{aligned} \quad (21)$$

where $\langle S_{ijkl} \rangle = \langle C_{ijkl} \rangle^{-1}$, $\langle C_{ijkl} \rangle = (1/V) \int_V C_{ijkl}(\mathbf{r}) dV$, $\langle \sigma_{ij}^0 \rangle = \frac{1}{V} \int_V C_{ijkl}(\mathbf{r}) \epsilon_{kl}^0(\mathbf{r}) dV$ and $\langle \delta\sigma_{ij} \rangle = \frac{1}{V} \int_V C_{ijkl}(\mathbf{r}) \delta\epsilon_{kl}(\mathbf{r}) dV$.

Thus our model can be applied to solve mechanical equilibrium equation in constrained as well as unconstrained systems.

2.3. Microstructural evolution

For a static grain structure, the position-dependent elastic stiffness tensor $C_{ijkl}(\mathbf{r})$ is evaluated once using equation (1). However, for an evolving grain structure $C_{ijkl}(\mathbf{r})$ is evaluated at every time step. Here we outline the governing equations for grain growth under an applied stress or strain. When elastic energy contribution is taken into account, the modified Cahn–Allen equation is given by

$$\frac{\partial \eta_g(\mathbf{r}, t)}{\partial t} = -L_g (\mu_{ch} + \mu_{el}), \quad (22)$$

where L_g is the relaxation coefficient, $\mu_{ch} = \delta F_{ch} / \delta \eta_g$, $\mu_{el} = \delta F_{el} / \delta \eta_g$, F_{ch} and F_{el} are the chemical and elastic parts of the free energy. μ_{ch} is given as

$$\mu_{ch} = \frac{\partial f(\eta_g)}{\partial \eta_g} - 2\kappa_g \nabla^2 \eta_g, \quad (23)$$

where $f(\eta_g)$ is the bulk free energy density and κ_g is the gradient energy coefficient associated with the order parameter field $\eta_g(\mathbf{r}, t)$. μ_{el} is obtained as

$$\begin{aligned} \mu_{el} &= \frac{\delta F_{el}}{\delta \eta_g} \\ &= \frac{\delta F_{el}}{\delta \eta_g^2} \cdot \frac{\delta \eta_g^2}{\delta \eta_g} = 2\eta_g \frac{\delta F_{el}}{\delta \eta_g^2}. \end{aligned} \quad (24)$$

If we ignore the modulus and volume differences between the grain boundaries and the interior, i.e. $C_{ijkl}(\mathbf{r})$ changes sharply across the grain boundaries and set $\epsilon_{ij}^0(\mathbf{r}) = 0$, the elastic driving force $\mu_{el}(\mathbf{r})$ is given by

$$\mu_{el}(\mathbf{r}) = \eta_g(\mathbf{r}) a_{ip}^g a_{jq}^g a_{kr}^g a_{ls}^g C_{pqrs} (\delta\epsilon_{ij}(\mathbf{r}) \delta\epsilon_{kl}(\mathbf{r}) + \bar{\epsilon}_{ij} \bar{\epsilon}_{kl} + 2\delta\epsilon_{ij}(\mathbf{r}) \bar{\epsilon}_{kl}), \quad (25)$$

where $\eta_g(\mathbf{r}) = 1$ within grain ‘g’ and zero elsewhere. The modified governing equation for grain growth is used to study migration of grain boundaries under applied stress in elastically inhomogeneous polycrystals.

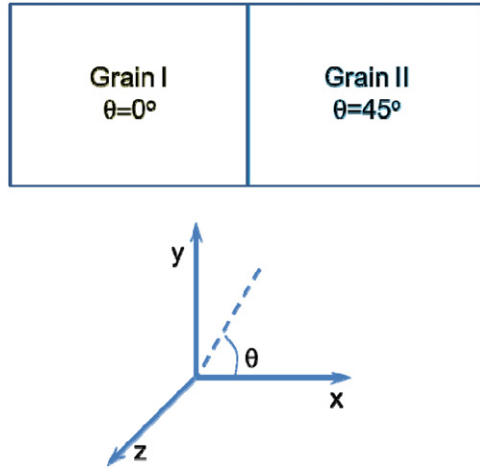


Figure 1. Schematic of the bicrystalline simulation cell. The x -direction is normal to the grain boundary and the surfaces normal to the x -direction are stress-free. The right grain is rotated by an angle 45° with respect to the left grain. The cell is periodic along all three directions.

3. Results and discussion

The simulations of stress-driven migration of planar and curved grain boundaries are carried out by solving the modified Allen–Cahn equation (equation (22)). The mechanical equilibrium equation (equation (7)) is solved in the reciprocal space to obtain μ_{el} . The time-dependent Allen–Cahn equation is then solved using a finite difference scheme. Periodic boundary conditions are employed in the simulations. The parameters used in our simulations are non-dimensionalized using characteristic length, time and energy units. In what follows, we present the values of all the parameters in their dimensionless form.

To gain useful insight into the mechanism of grain boundary movement, we considered bicrystalline systems containing planar and curved grain boundaries. We further extended our study to general multigrain systems. In all the examples given below, the homogeneous strain (i.e. the macroscopic strain) and the elastic energy density are calculated using the following assumptions: (i) the elastic modulus changes sharply across the grain boundaries (i.e. no modulus difference between the grain boundaries and the interior) and (ii) the excess volume associated with the grain boundaries is zero (i.e. no volume difference between the grain boundaries and the interior).

First, we consider a bicrystal separated by a planar grain boundary. The simulation cell geometry and coordinate system are shown schematically in figure 1. The grains are oriented at 0° and 45° , respectively, with respect to a fixed reference frame. In other words, the misorientation angle between the two grains is 45° . The two grains are described using two order parameters, $\eta_1(\mathbf{r}, t)$ and $\eta_2(\mathbf{r}, t)$, respectively, such that $\eta_1 = 1$, $\eta_2 = 0$ within grain I and $\eta_1 = 0$, $\eta_2 = 1$ within grain II. η_1 and η_2 have finite non-zero values at the grain boundary. Grain boundary migration under applied strain/stress is described by solving the temporal evolution equations for $\eta_1(\mathbf{r}, t)$ and $\eta_2(\mathbf{r}, t)$.

The simulation cell is assumed to be periodic along all three directions. The cell is then subjected to a biaxial applied strain, $\epsilon_{yy} = \epsilon_{zz} = 0.01$, while the directions normal to the x -axis are assumed to be stress free, i.e. $\sigma_{xx} = \sigma_{yx} = \sigma_{zx} = 0$. We have assumed the bicrystal to be elastically anisotropic with cubic elastic constants, $C_{11} = 450$, $C_{12} = 150$, $C_{44} = 300$.

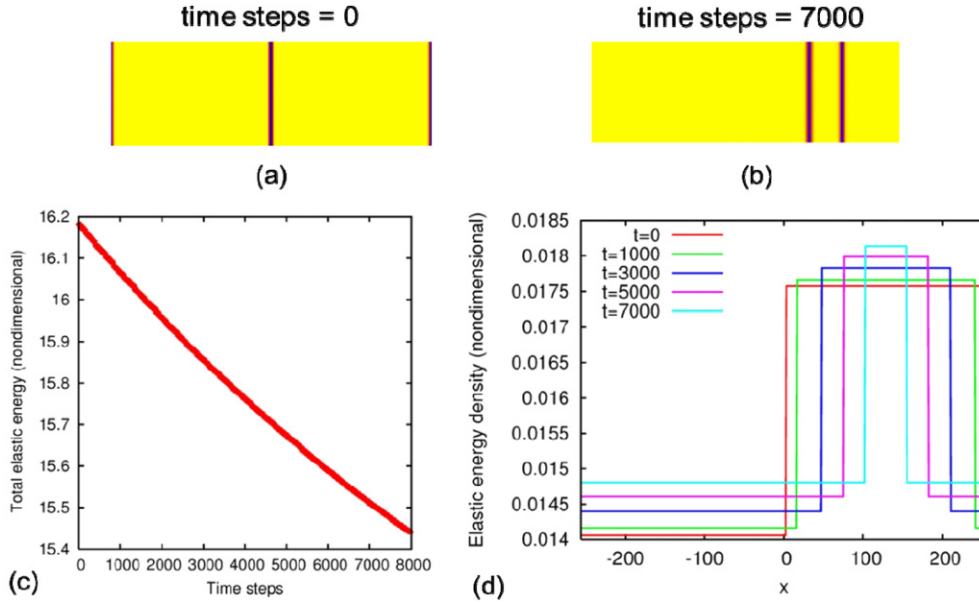


Figure 2. (a), (b) Time snapshots of grain boundary motion when the simulation cell is subjected to biaxial strain $\epsilon_{yy} = \epsilon_{zz} = 0.01$. The boundaries normal to the x -axis are stress free, i.e. $\sigma_{xx} = \sigma_{yx} = \sigma_{zx} = 0$. (c) Total elastic energy of the bicrystalline system subjected to biaxial strain as a function of time. (d) Elastic energy density profiles plotted across the grain boundary at different times during migration.

If the bicrystal is assumed to be elastically isotropic, the elastic driving force to move the grain boundary is zero. The simulation geometry is similar to the one described by Zhang *et al* [8] for their study of elastically driven grain boundary migration using MD simulations, except for the fact that we assume periodic boundary conditions along all three directions.

We observed that the addition of elastic energy leads to the reduction of the equilibrium values of order parameters within each grain, which in turn affects the elastic energy density within each grain. This problem can be alleviated if we make $\mu_{el}(\mathbf{r})$ dependent on a function $H(\eta)$ instead of η such that the value of the function is always maintained at the equilibrium values 0 and 1 within the bulk of each grain.

$H(\eta)$ is defined as follows: $H(\eta) = 2\eta^3 - 3\eta^2$; $H(\eta) = 0$ when $\eta = 0$; $H(\eta) = 1$ when $\eta = 1$; and $\partial H/\partial \eta = 0$ when $\eta = 0, 1$.

Under applied biaxial strain, the grain boundary movement at two different times is shown in figures 2(a) and (b). The boundary moves toward the grain oriented at 45° (designated as grain II). Finally, the unfavorably oriented grain (grain II) dissolves under the action of a biaxial applied strain. The boundary moves in such a way as to decrease the total elastic energy of the system (figure 2(c)). Elastic energy density profiles across the grain boundary at different times are shown in figure 2(d). At any given time, the elastic energy density is constant within each grain and increases sharply from grain I to grain II. In this case, the difference between the stored elastic energy densities between the two grains provides the driving force for grain boundary migration:

$$\Delta F = F_e^{\text{II}} - F_e^{\text{I}}, \quad (26)$$

where ΔF represents the elastic driving force, F_e^{I} , F_e^{II} are the elastic energy densities in grains I and II, respectively.

The grain with lower elastic energy density grows at the expense of the grain with higher elastic energy density. In this particular case, the driving force remains roughly constant through the entire simulation except at the very late stages when the driving force decreases with time. The reduction in driving force at the late stages is an artifact of the periodic boundary conditions and finite system size employed in our simulations. When the energetically unfavorable grain disappears from the system, the grain boundaries tend to merge causing the driving force to reduce. This is why the relationship between the total elastic energy and time steps becomes nonlinear at the late stages (figure 2(c)). The velocity of the grain boundary (v) is measured to be a constant (2.23×10^{-4}) in nondimensional units). From the simulations, the average driving force is found to be 0.01426 (in nondimensional units). The mobility of the grain boundary (M) is estimated to be 0.01564 by assuming that the velocity is linearly proportional to the driving force ($v = M \Delta F$). The mobility can also be defined as the derivative of velocity with respect to driving force in the small driving force limit [8]:

$$M = \left(\frac{\partial v}{\partial \Delta F} \right)_{\Delta F=0}. \quad (27)$$

Using linear elasticity, the difference in stored energy densities between the two grains is given by [8]:

$$\Delta F = \frac{(C_{11} - C_{12})(C_{11} + 2C_{12})^2 C_a \sin^2(2\theta)}{C_{11}[4C_{11}(C_{11} - C_{12} + C_a) - (C_{11} + C_{12})C_a(1 - \cos(4\theta))]} \epsilon^2, \quad (28)$$

where θ represents the misorientation between the two bounded grains, ϵ is the magnitude of applied strain, $C_a = 2C_{44} - C_{11} + C_{12}$ is a measure of anisotropy in the system. Plugging in the elastic constants and the misorientation angle in equation (28) we obtain the driving force to be 0.015625 (nondimensional units). Thus we obtain good agreement between the analytically obtained driving force and that obtained from the simulation.

We also compared the elastic energy density and the elastic potential (defined by $\Delta f_e = (C_{ijkl}^I - C_{ijkl}^{II}) \epsilon_{ij}^{el}(\mathbf{r}) \epsilon_{kl}^{el}(\mathbf{r})$) when an elastically anisotropic bicrystalline system is subjected to a uniaxial applied stress, perpendicular and parallel to the grain boundary, respectively. The elastic constants of the system are assumed to have cubic symmetry ($C_{11} = 450$, $C_{12} = 150$, $C_{44} = 300$). The anisotropy parameter $A_Z (= 2C_{44}/(C_{11} - C_{12}))$ is 3 which indicates that the $\langle 100 \rangle$ directions are the elastically soft directions. The temporal evolutions of elastic energy density and elastic potential when stress $\sigma_{xx}^a = 1.5$ is applied normal to the grain boundary are shown in figures 3(a) and (b). In this case, the stored elastic energy density in grain I is larger than in grain II, although the former is growing and the latter is shrinking with time (figure 3(a)). However, if we take into account the elastic potential profiles, the advancing grain I has a lower elastic potential than the shrinking grain II (figure 3(b)). On the other hand, when stress is applied parallel to the grain boundary, both the elastic energy density and elastic potential are lower in the advancing grain I than the shrinking grain II (figures 3(c) and (d)). Thus, we may infer that the difference in elastic potential between the two grains is a more appropriate measure of the mechanical driving force.

The stress distributions $\sigma_{xx}(\mathbf{r})$, $\sigma_{xy}(\mathbf{r})$ and $\sigma_{yy}(\mathbf{r})$ are also compared in these two cases. In both cases, the shear stress component within both the grains is zero throughout the simulation. This is a sufficient condition to prevent grain boundary sliding. When stress is applied normal to the boundary, $\sigma_{xx}(\mathbf{r}) = \sigma_{xx}^a = 1.5$ in the entire system. However, the distribution of $\sigma_{yy}(\mathbf{r})$ is significantly different within grains I and II: $\sigma_{yy}(\mathbf{r})$ is tensile (positive) in grain I and compressive (negative) in grain II. As time progresses, $\sigma_{yy}(\mathbf{r})$ decreases to zero within grain I with the decrease in the area of grain II (figures 4(a) and (b)). When the system is subjected to an uniaxial stress parallel to the boundary ($\sigma_{yy}^a = 1.5$ and all other stress components are zero), $\sigma_{xx}(\mathbf{r}) = 0$ within each grain. Similar to the previous example, the boundary migrates toward

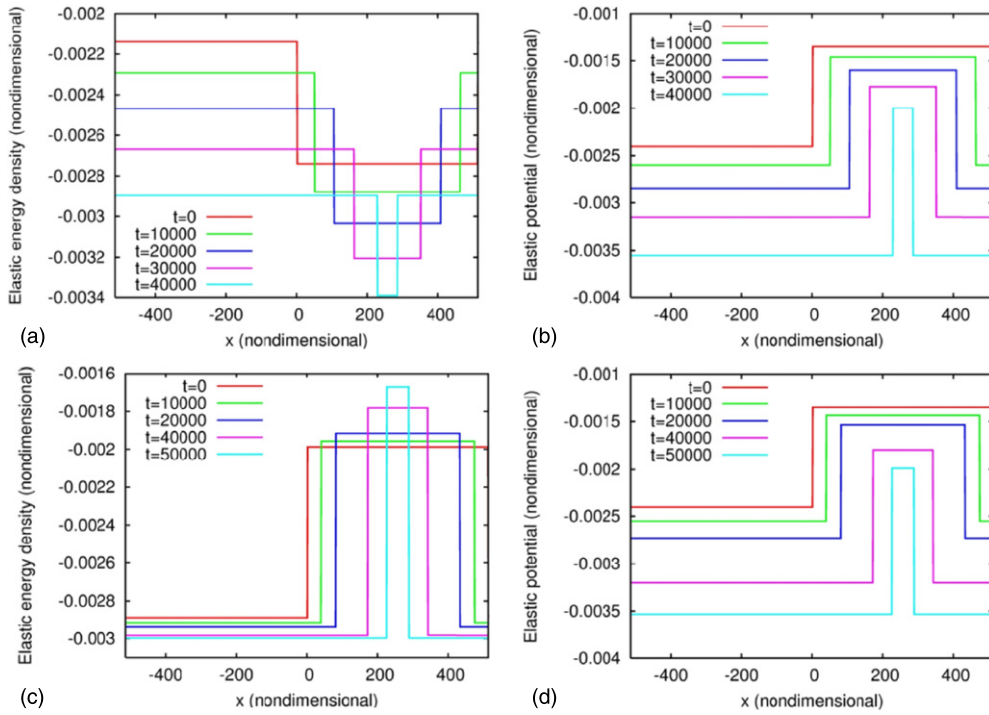


Figure 3. (a), (b) Elastic energy density and elastic potential profiles plotted across the grain boundary at different times during migration when a bicrystal is subjected to a uniaxial stress $\sigma_{xx}^a = 1.5$ normal to the boundary. (c), (d) Elastic energy density and elastic potential profiles plotted across the grain boundary at different times during migration when a bicrystal is subjected to a uniaxial stress $\sigma_{yy}^a = 1.5$ parallel to the boundary.

grain II leading to its shrinkage. However, in this case, $\sigma_{yy}(r)$ is positive (tensile) in both grains and the magnitude of $\sigma_{yy}(r)$ is larger in grain II than in grain I (figures 4(c) and (d)). As grain II shrinks the overall elastic energy of the system decreases. The comparison of the stress distributions suggests that two different mechanisms are in play when stress is applied normal or parallel to the boundary.

The mechanical driving force for migration (given by the difference in elastic potential) of a planar grain boundary is plotted as a function of time in figure 5(a) when the boundary is subjected to uniaxial applied stress, perpendicular or parallel to the boundary. In both cases, the driving force for grain boundary migration increases with increasing time. During the early transient stages, the driving force changes nonlinearly with time. When steady state is achieved, the variation of driving force with time is almost linear. In both cases, the velocity of migration is plotted versus the driving force in the steady-state regime (figure 5(b)). In the steady-state regime, the velocity changes linearly with the driving force. The constant of proportionality (i.e. the mobility) is obtained from the slopes of the lines. The lines are almost parallel which suggests that the value of mobility is independent of the direction of applied stress. However, if the magnitude of applied stress is small, the extent of transient regime is larger. Moreover, at the very late stages, we observe some nonlinearity in the velocity-driving force relation which may be an artifact of the periodic boundary conditions.

It should be noted that Winning *et al* [4, 5] proposed a model where the grain boundaries are modeled as dislocation networks and the grain boundary movement was caused by the

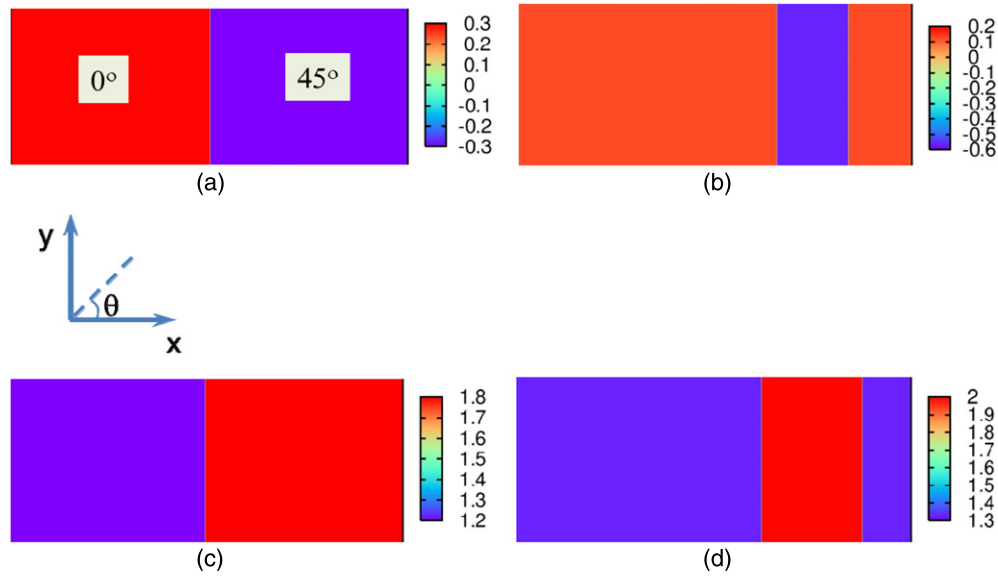


Figure 4. (a), (b) Distribution of $\sigma_{yy}(r)$ at two different time steps when a bicrystal with a planar boundary is subjected to uniaxial stress normal to the grain boundary (along the x -axis). (c), (d) Distribution of $\sigma_{yy}(r)$ at two different time steps when a bicrystal with a planar boundary is subjected to uniaxial stress parallel to the grain boundary (along the y -axis).

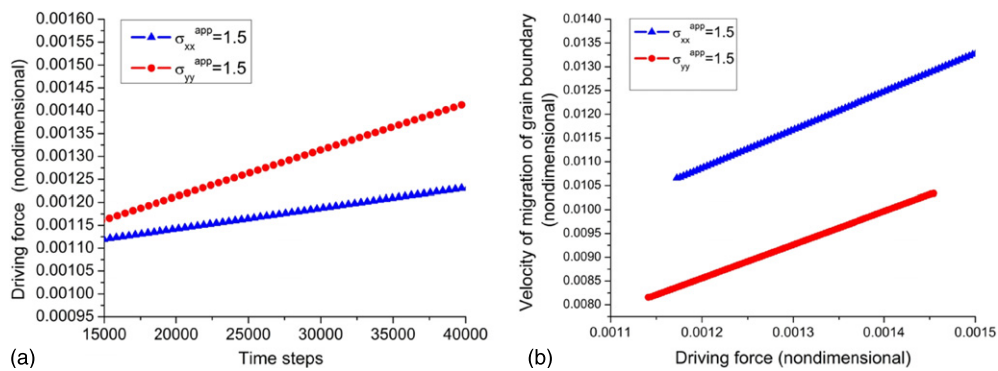


Figure 5. (a) Driving force for grain boundary migration versus time in the steady-state regime. (b) Grain boundary migration velocity plotted as a function of driving force in the steady-state regime. In both figures, the blue triangles and red circles correspond to the systems where stress is applied normal and parallel to the grain boundary, respectively. In both systems, the velocity versus driving force curves are linear and are nearly parallel to each other indicating a similar mobility of the boundary.

movement of dislocations under shear stress. However, in our model we propose that the difference in elastic stiffness of the misoriented grains in the direction of loading provides a bulk mechanical energy difference which causes the grain boundaries to move.

We also studied the effect of applied stress on the motion of curved boundaries. For this purpose we chose a bicrystalline system in which a circular grain (grain I) is placed at the center of the simulation box surrounded by a differently oriented grain (grain II). The relative orientations of grain I and grain II are 0° and 45° , respectively, with respect to a fixed

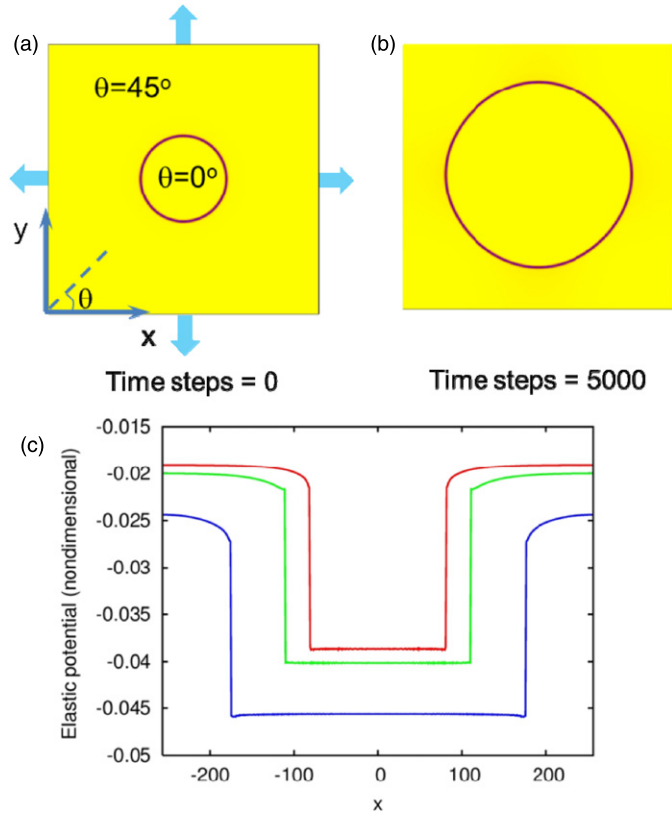


Figure 6. (a) Schematic of the bicrystalline simulation cell containing a curved boundary. The central circular grain is oriented at 0° and the surrounding grain is oriented at 45° with respect to a fixed reference frame. (b) The elastically soft circular grain grows when subjected to applied pressure. (c) Elastic potential profiles drawn along a radial direction at various times during migration of the curved boundary.

reference frame. The initial configuration of the system is shown schematically in figure 6(a). We first assume both grains to be elastically isotropic with the circular grain being elastically softer than the surrounding grain. In terms of elastic properties, the system is similar to a two-phase system containing grains with different orientation. The elastic constants of grain II are $C_{11} = 450$, $C_{12} = 150$ while the elastic constants of the central grain I is assumed to be $C_{11} = 225$, $C_{12} = 75$. The system is then subjected to an applied pressure $\sigma_{xx}^a = \sigma_{yy}^a = 1.5$ with other stress components being zero. The elastically soft central grain grows under the application of pressure (see figure 6(b)). In this case, there are two competing factors affecting the growth or shrinkage of the circular grain: (a) driving force due to interfacial curvature which causes the circular grain to shrink and (b) driving force due to reduction in elastic energy of the system which causes the softer circular grain to grow. The critical radius of the circular grain, r_c , at which it begins to grow is obtained from a balance between the two driving forces:

$$r_c = \frac{\gamma}{\frac{\sigma_a^2}{E_1} - \frac{\sigma_a^2}{E_2}}, \quad (29)$$

where γ is the grain boundary energy, σ_a is the magnitude of applied pressure, E_1 and E_2 are Young's moduli for the circular grain and the surrounding grain, respectively. The critical

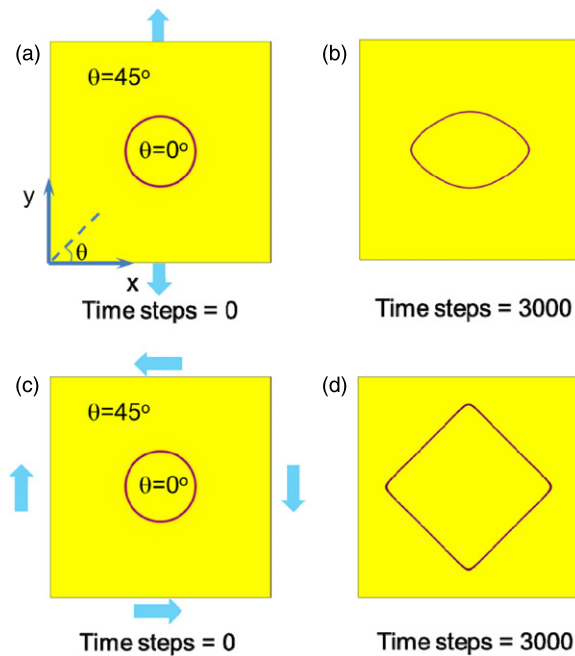


Figure 7. (a), (b) Time snapshots of grain boundary migration in an elastically anisotropic system with cubic symmetry containing a favorably oriented circular grain when the system is uniaxially stressed along the x -axis. (c), (d) Time snapshots of grain boundary migration in an elastically anisotropic system with cubic symmetry containing a favorably oriented circular grain when the system is subjected to shear. The solid arrows indicate the directions of applied load.

radius, r_c , is estimated to be 72 length units for our system. We have taken the initial radius of the circular grain to be greater than r_c . At this size the softer circular grain can overcome the shrinkage force due to curvature and continue to grow under applied pressure. The elastic potential of the circular grain is lower than the surrounding grain (shown in figure 6(c)). The difference in elastic potential provides the mechanical driving force for the circular grain to grow.

In the previous case, we assumed the system to be elastically isotropic and inhomogeneous. However, the system can also be elastically anisotropic, which may further increase the mechanical driving force due to reduction in elastic energy, and may also lead to shape change of the circular grain under applied stress. In an elastically anisotropic system, when the applied loading direction favors the growth of a grain with positive curvature, the grain will continue to grow and change its shape once its size exceeds the critical size. For example, figure 7(a) shows the growth of a circular grain (with a misorientation angle of 0° w.r.t. a fixed reference frame) surrounded by another grain (with a misorientation angle of 45° w.r.t. a fixed reference frame) in an elastically anisotropic system with cubic symmetry (in which $\langle 10 \rangle$ directions are the elastically soft directions), when the system is subjected to a uniaxial applied stress along the x -axis. During growth, the circular grain changes its shape to elliptical with its long axis perpendicular to the direction of applied stress. In another example, we observe the growth of the favorably oriented central circular grain into a square shape under the application of shear (figure 7(b)).

Our model is also applied to study the migration of grain boundaries in multigrain systems. Although our model can be applied to study grain growth in complex polycrystalline systems

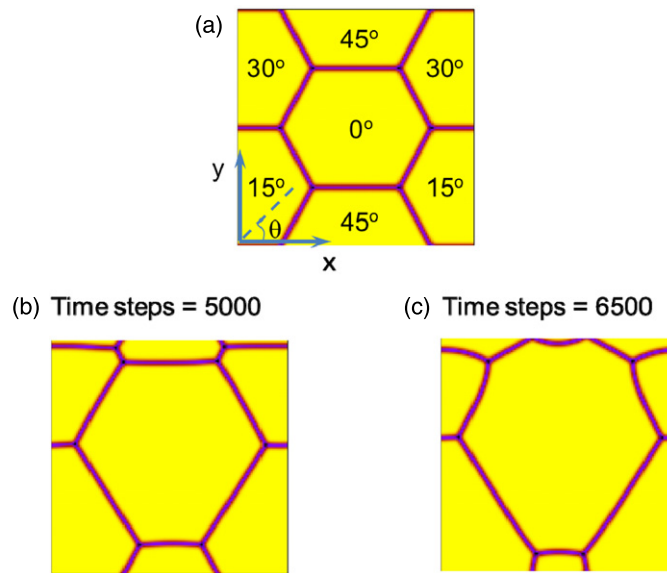


Figure 8. (a) A two-dimensional multigrain system subjected to applied stress along the y -axis. Initially, all the grain boundaries are planar. (b), (c) Time snapshots of grain boundary migration in the multigrain system.

containing several thousand grains, we provide a much simpler example of a multigrain system containing four grains with cubic symmetry. In this system, a misorientation angle of 0° with respect to a fixed reference frame is assigned to the central grain, while the surrounding grains are assigned different orientations and the boundaries between the central grain and the surrounding grains are assumed to be high-angle grain boundaries. The system is subjected to an applied stress $\sigma_{yy}^a = 3.0$, all other stress components being zero. The system considered is shown in figure 8(a).

The evolution of the grain structure subjected to applied stress is shown in figures 8(b) and (c). The grain boundary energy is assumed to be isotropic. Initially the boundaries are planar (i.e. there is no driving force due to curvature). On the application of stress, the grain at the center starts growing and the boundaries enveloping the grain develop negative curvature. Since the central grain is favorably oriented with respect to the direction of applied stress, it grows into the surrounding grains by developing negative curvature at the boundaries. The local stress fields at an intermediate time are shown in figure 9. We observe that the local stress distributions depend crucially on the relative misorientation of the neighboring grains. As a consequence, the central grain grows at different rates along different directions.

In the case of the multigrain system, we show that application of stress may induce negative curvature of the grain boundaries. Our study of multigrain systems is currently being extended to more complex large-scale systems in two and three dimensions and will be reported elsewhere.

4. Conclusions

We developed a phase-field model to study stress-driven grain boundary migration in elastically inhomogeneous polycrystals. We studied the stress effect on migration of planar and curved grain boundaries. We observe that the boundary mobility depends crucially on the

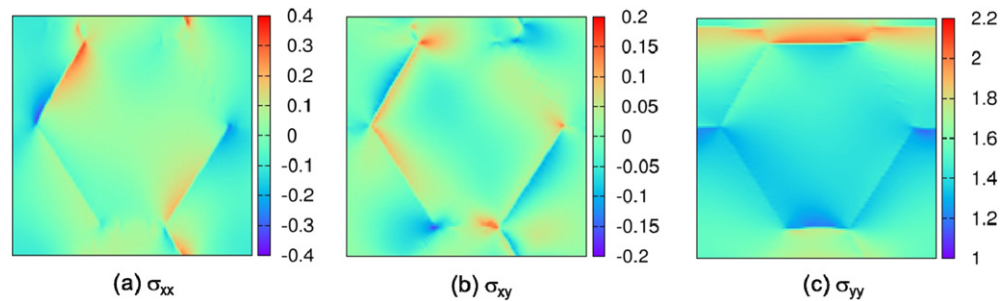


Figure 9. (a), (c) Local stress distributions $\sigma_{xx}(\mathbf{r})$, $\sigma_{xy}(\mathbf{r})$, $\sigma_{yy}(\mathbf{r})$ at an intermediate time step = 5000.

misorientation between the grains, but is independent of the direction of the applied load in the steady-state regime. The mobility value obtained from our study of planar grain boundaries agrees well with the analytical solution. In the case of curved boundaries, application of stress may not only induce migration of the boundaries opposing the driving force due to curvature but may also cause the grain shape to change in elastically anisotropic systems. We observe that applied stress can induce negative curvature of boundaries in a preferentially oriented grain which may eventually lead to abnormal grain growth.

Acknowledgment

The authors would like to acknowledge the financial support from the National Science Foundation under the grant number DMR-0710483.

References

- [1] Gottstein G and Shvindlerman L 1999 *Grain Boundary Migration in Metals: Thermodynamics, Kinetics, Applications* (Boca Raton, FL: CRC)
- [2] Bainbridge D, Choh H and Hedwards E 1954 Recent observations on the motion of small angle dislocation boundaries *Acta Metall.* **2** 322–33
- [3] Li C *et al* 1953 Stress-induced movement of crystal boundaries *Acta Metall.* **1** 223–9
- [4] Winning M, Gottstein G and Shvindlerman L S 2001 Stress induced grain boundary motion *Acta Mater.* **49** 211–9
- [5] Winning M, Gottstein G and Shvindlerman L S 2002 On the mechanisms of grain boundary migration *Acta Mater.* **50** 353–63
- [6] Molodov D, Ivanov V and Gottstein G 2007 Low angle tilt boundary migration coupled to shear deformation *Acta Mater.* **55** 1843–8
- [7] Schönfelder B *et al* 1997 Molecular-dynamics method for the simulation of grain-boundary migration *Interface Sci.* **5** 245–62
- [8] Zhang H, Mendelev M I and Srolovitz D J 2004 Computer simulation of the elastically driven migration of a flat grain boundary *Acta Mater.* **52** 2569–76
- [9] Ivanov V A and Mishin Y 2008 Dynamics of grain boundary motion coupled to shear deformation: an analytical model and its verification by molecular dynamics *Phys. Rev. B* **78** 064106
- [10] Mishin Y, Asta M and Li J 2010 Atomistic modeling of interfaces and their impact on microstructure and properties *Acta Mater.* **58** 1117–51
- [11] Fratzl P, Penrose O and Lebowitz J 1999 Modeling of phase separation in alloys with coherent elastic misfit *J. Stat. Phys.* **95** 1429–503
- [12] Chen L Q and Wang Y 1996 The continuum field approach to modeling microstructural evolution *JOM* **48** 13–18
- [13] Chen L 2002 Phase-field models for microstructure evolution *Annu. Rev. Mater. Res.* **32** 113–40
- [14] Chen L and Yang W 1994 Computer simulation of the domain dynamics of a quenched system with a large number of nonconserved order parameters: the grain-growth kinetics *Phys. Rev. B* **50** 15752–6

- [15] Fan D and Chen L-Q 1997 Computer simulation of grain growth using a continuum field model *Acta Mater.* **45** 611–22
- [16] Kobayashi R, Warren J A and Carter W C 1998 Vector-valued phase field model for crystallization and grain boundary formation *Physica D* **119** 415–23
- [17] Kazaryan A *et al* 2000 Generalized phase-field model for computer simulation of grain growth in anisotropic systems *Phys. Rev. B* **61** 14275–8
- [18] Jou H J, Leo P H and Lowengrub J S 1997 Microstructural evolution in inhomogeneous elastic media *J. Comput. Phys.* **131** 109–48
- [19] Moulinec H and Suquet P 1998 A numerical method for computing the overall response of nonlinear composites with complex microstructure *Comput. Methods Appl. Mech. Eng.* **157** 69–94
- [20] Michel J, Moulinec H and Suquet P 1999 Effective properties of composite materials with periodic microstructure: a computational approach *Comput. Methods Appl. Mech. Eng.* **172** 109–43
- [21] Michel J C, Moulinec H and Suquet P 2001 A computational scheme for linear and non-linear composites with arbitrary phase contrast *Int. J. Numer. Methods Eng.* **52** 139–60
- [22] Lebensohn R A 2001 N-site modeling of a 3D viscoplastic polycrystal using fast Fourier transform *Acta Mater.* **49** 2723–37
- [23] Wang Y, Jin Y and Khachaturyan A 2002 Phase field microelasticity theory and modeling of elastically and structurally inhomogeneous solid *J. Appl. Phys.* **92** 1351–60
- [24] Wang Y, Jin Y and Khachaturyan A 2002 Three-dimensional phase field microelasticity theory of a complex elastically inhomogeneous solid *Appl. Phys. Lett.* **80** 4513
- [25] Hu S Y and Chen L Q 2001 A phase-field model for evolving microstructures with strong elastic inhomogeneity *Acta Mater.* **49** 1879–90
- [26] Yu P *et al* 2005 An iterative-perturbation scheme for treating inhomogeneous elasticity in phase-field models *J. Comput. Phys.* **208** 34–50
- [27] Zhu J, Chen L-Q and Shen J 2001 Morphological evolution during phase separation and coarsening with strong inhomogeneous elasticity *Modelling Simul. Mater. Sci. Eng.* **9** 499
- [28] Fan D, Geng C and Chen L Q 1997 Computer simulation of topological evolution in 2-D grain growth using a continuum diffuse-interface field model *Acta Mater.* **45** 1115–26
- [29] Khachaturyan A G 1983 *Theory of Structural Transformations in Solids* (New York: Wiley)
- [30] Li D Y and Chen L Q 1998 Shape evolution and splitting of coherent particles under applied stresses *Acta Mater.* **47** 247–57